



المجلة العلمية لجامعة الملك فيصل The Scientific Journal of King Faisal University

العلوم الأساسية والتطبيقية
Basic and Applied Sciences



Tuning of Morphological, Structural and Optical Properties of α -Fe₂O₃ Nanoparticles by Precursor Concentration

Adil Alshoabi

Department of Physics, College of Science, King Faisal University, Al Ahsa, Saudi Arabia

التحكم بالخواص الضوئية والتركيبية للحبيبات النانوية لأكسيد الحديد الهيماتيت باستخدام التركيزات

عادل الشعبي

قسم الفيزياء، كلية العلوم، جامعة الملك فيصل، الأحساء، المملكة العربية السعودية

KEYWORDS

الكلمات المفتاحية

Band gap energy, green synthesis, hematite iron oxide, X-ray diffraction
طاقة الفجوة، الحبيبات النانوية، أكسيد الحديد الهيماتيت، حيود أشعة إكس

RECEIVED

الاستقبال

11/08/2020

ACCEPTED

القبول

30/09/2020

PUBLISHED

النشر

01/12/2020



<https://doi.org/10.37575/bj/sci/0018>

ABSTRACT

The current study focuses on a dual aim of developing an easy method to synthesise monodisperse hematite iron oxide (α -Fe₂O₃) nanoparticles and controlling their optical, structural and morphological properties. By using a low-cost and eco-friendly room temperature sonication method, a series of iron oxide nanoparticles were prepared on a nano scale, with fine sizes ranging from 4–10 nm. Optical, structural and morphological properties were precisely modified by varying the concentration of the solution of iron chloride (0.01 M, 0.02 M and 0.05 M). X-ray diffraction and Raman spectra revealed that the prepared nanoparticles had a high crystallinity, confirming that they were hematite. The nanoparticles' crystallite sizes increased from 6 to 10 nm with solution molarity. The optical measurements showed that the band gap energy of α -Fe₂O₃ nanoparticles (annealed) decreased from 2.67 eV to 2.46 eV with the increasing of solution molarity from 0.01 M to 0.05 M, respectively. Results of field emission scanning electron microscopy demonstrated that the α -Fe₂O₃ nanoparticles appeared as spherical dots, and their sizes increased from 6 to 10 nm with the concentration of the solution. The presented green synthesis might be useful in controlling the functional properties of magnetic nanostructures for a variety of applications.

المخلص

في الدراسة الحالية، تم تحضير حبيبات متناهية في الصغر في حجم 4-10 نانومتر باستخدام طريقة رخيصة الثمن وقليلة التكلفة وصديقة للبيئة عن طريق الموجات الصوتية، وباستخدام تغيير تركيز نترات الحديد، تم التحكم في الخواص الضوئية والتركيبية. نتاج حيود أشعة إكس وضحت وأكدت أن المنتج عالي البلورة ومكون من حبيبات في حجم النانو من نوع الهيماتيت. حجم الحبيبات كان يتراوح بين 4-8 نانومتر، وبالمعالجة الحرارية تم زيادة حجم البلورات لتكون في مدى 6-10 نانومتر. القياسات الضوئية أظهرت أن طاقة الفجوة للحبيبات النانوية 2.67 إلكترون فولت. وبالتحكم في تركيز نترات الحديد، تم تقليل طاقة الفجوة إلى 2.46 إلكترون فولت. نتاج الميكروسكوب الإلكتروني الماسح أظهرت أن الحبيبات النانوية لها شكل دائري وأكدت أن حجم الحبيبات النانوية يمكن التحكم بها بين 6 نانومتر إلى 10 نانومتر اعتماداً على التركيزات. في النهاية، يمكن استخلاص أن طرق التحضير الخضراء تكون مفيدة في التحكم في الخواص الوظيفية للتركيبات النانوية المغناطيسية وبالتالي تكون متاحة لتطبيقات صناعية واسعة.

1. Introduction

Hematite (α -Fe₂O₃) considers one of n-type semiconductors with band gap energy around 2.1 eV, which becomes one of the good stable phases thermodynamically of Fe₂O₃ family. It is an inexpensive magnetic material and has environmentally benign properties. Hematite has been widely used in numerous applications including magnetic recording media, gas sensors catalysts, lithium ion batteries, biomedicine and bio-diagnostics due to its nontoxic nature, cost effectiveness, and high corrosion resistance (Chen *et al.*, 2010; Cherian *et al.*, 2012; Horak *et al.*, 2017; Khabiri *et al.*, 2020; Khatami *et al.*, 2019; Patil *et al.*, 2018; Ramalingam *et al.*, 2020; Wang *et al.*, 2012; Widayat *et al.*, 2019; Xia *et al.*, 2018; Zhu *et al.*, 2010). Generally, the (nano/micro) materials properties are strongly linked to their morphology and size (Xia *et al.*, 2009). For the utilization of various technological applications, the adjustment of their sizes, shapes and porosity was intensively followed.

Numerous methods have been used for preparing iron oxides nanoparticles (Ibrahim *et al.*, 2018; Lubis *et al.*, 2018; Mufti *et al.*, 2014; Qiu *et al.*, 2011; Rasheed *et al.*, 2016). In the same trend, chemical precipitation, (Sivakumar *et al.*, 2014) solid-state reaction, (Li *et al.*, 2014) hydrothermal method, (Xu *et al.*, 2015) sol-gel method, (Kopanja *et al.*, 2016) and pyrolytic process (Chen *et al.*, 2010) have been used for developing iron oxide nanostructures. However, these synthesis routes appear to be inopportune because of the requirement of complete template removal, high cost and long synthesis cycle in addition to low yield and large amount of solvents as shown in the sol-gel method and micro-emulsion process (Tao *et al.*, 2020). Also, the elimination of the surfactants or shape-control ions is not favorable for the morphology of the final products

(Bondarchuk *et al.*, 2017; Zhou *et al.*, 2020). Moreover, the previously mentioned synthetic routes required longer reaction time, high temperature and pressure, high cost and poor safety performance in addition to complicated steps as seen in the hydrothermal techniques and solid-state reactions. In the chemical precipitation process, there are serious agglomerations of particles leading to application limit and wide particle size distribution (Patil *et al.*, 2018; Ren *et al.*, 2017; Ryan *et al.*, 2017).

Therefore, it is essential to develop a simple and adaptable method for preparing α -Fe₂O₃ nanostructures with tunable sizes. As compared with other synthesis methods, due to its simplicity, and large-scale production feasibility, the solution-based synthesis technique is more attractive. For the growth of α -Fe₂O₃ nanostructures, ultra-sonication synthesis has been shown to be an adaptable method because of its low processing temperature, mass production, high quality, cost effective and environmental benign nature.

In this trend, the current study has used a simple sonication synthesis method for synthesizing α -Fe₂O₃ nanoparticles. Their structural, optical, and morphological properties can be easily tuned by the solution concentration. X-ray diffraction, field emission scanning electron microscopy and Raman spectroscopy have used to characterize the prepared nanomaterials. The optical properties were measured and used for calculating the band gap energy for the prepared nanostructures.

2. Materials and Methods

A simple sonication method was used for synthesizing α -Fe₂O₃ nanoparticles. Analytically pure reagents (A. R.) of FeCl₃·6H₂O (purity \geq

98%) has been dissolved in de-ionized water (DIW) for forming an aqueous solution at various concentrations: 0.01, 0.02 and 0.05 M of iron chloride. The reaction solution in a beaker was then transferred to an ultrasonication system at room temperature. The reaction has been accomplished for 30 min by adding ammonia (approximately 30%) to the solution at pH=4. After the reaction was completed, α -Fe₂O₃ precursors were precipitated, which was then washed thoroughly few times with ethanol and water. The product was filtrated, dried and grounded. The dried product calcined at 400 °C for 2 hours in a muffle furnace.

X-ray diffraction (XRD) was used to characterize the prepared materials by using X-ray diffractometer, Philips X'PERT MPD PW3040 equipped with Cu K α radiation at $\lambda=1.5406 \text{ \AA}$, operating at a current value of 30 mA and a voltage value of 40 kV. The XRD patterns were recorded in the scan ranging from 30° to 65° of 2 θ under a step size of 0.02° with scan speed of 2 θ /min. Images of field emission scanning electron microscopy (FE-SEM) were collected using a JEOL microscope. A (UV-Vis) spectrophotometer (Shimadzu) was used to measure the room temperature optical absorption spectrum ranging from 200–800 nm. Phonon vibrational measurements of α -Fe₂O₃ nanostructures were carried out by using micro-Raman spectrometer (Renishaw) with an excitation source of 532-nm of (SSL) solid state primary laser.

3. Results and Discussion

The XRD patterns of α -Fe₂O₃ nanoparticles without calcinations were illustrated in Figure 1. It can be seen that the samples of low concentrations (0.01 M and 0.02 M) consist of large amorphous phases. Whereas the characteristic peaks of α -Fe₂O₃ were observed in the high concentration. The clear broad peaks indicated that minute crystalline α -Fe₂O₃ is clearly formed in the solution process at RT.

Figure 1. XRD patterns of as-prepared α -Fe₂O₃ nanoparticles.

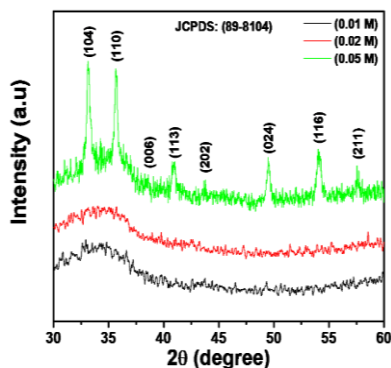
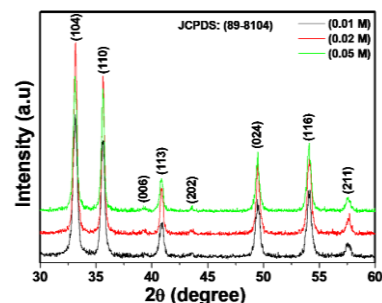


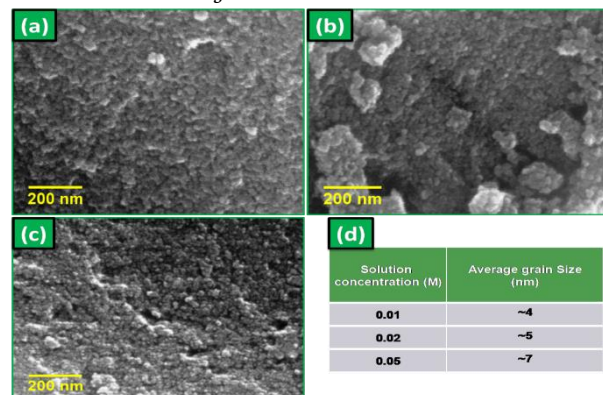
Figure 2. XRD patterns of α -Fe₂O₃ nanoparticles calcined at 400 °C for 2 h.



Calculated values of average crystallite size of as-prepared α -Fe₂O₃ nanoparticles estimated according to the Scherer equation was found to be ~4 nm, ~5 nm, ~7 nm. After being calcined at 400 °C for 2 h, there is an evident crystallization as shown in the XRD patterns of α -Fe₂O₃ nanoparticles in Figure 2. The process of crystallization are

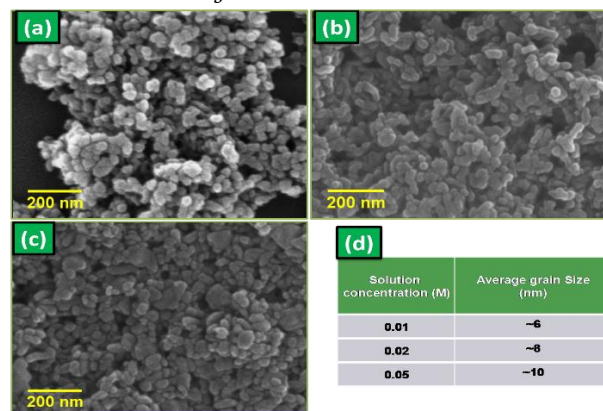
well-established at 400 °C with enhancing intensities of some primary peaks and appearing new diffraction peaks. Within the XRD detection limit, it was clear that all the diffraction peaks obtained for all these samples are well matched to the diffraction pattern of the standard JCPDS card No. 89-8104 of pure rhombohedral symmetry of hematite Fe₂O₃ (Ahmed *et al.*, 2014). No impurity peaks were observed in the diagrams. The sharp and strong diffraction peaks illustrated a high degree of crystallization of α -Fe₂O₃ nanostructures. Collected values of average crystallite size of the calcined nanoparticles obtained using the Scherer equation was found to be ~6 nm, ~8 nm, ~10 nm for 0.01, 0.02, and 0.05 M concentration, respectively. These results indicated that increasing concentration of iron chloride lead to improve the crystallization of as-synthesized products.

Figure 3. FESEM images of without calcined α -Fe₂O₃ nanoparticles with various concentration of (a) 0.01 M (b) 0.02 M, (c) 0.05 M, and (d) table showing the variation of grain size with concentration.



Figures 3 (a-c) demonstrates the FE-SEM images of α -Fe₂O₃ with 0.01, 0.02, and 0.05 M concentration without calcined (as prepared). It is obvious from Figure 3(a) that the agglomerated fine particles of α -Fe₂O₃ have an average diameter of ~4 nm, while for 0.02 M, the average diameter of ~5 nm (see Figure 3(b)), and for 0.05 M, diameter of ~7 nm (see Figure 3(c)), respectively. These images indicate that crystallization was not completely occurred, which resulted to agglomerate particles with smaller size. Interestingly, after the calcinations, evident change in morphology was observed as shown in Figure 4.

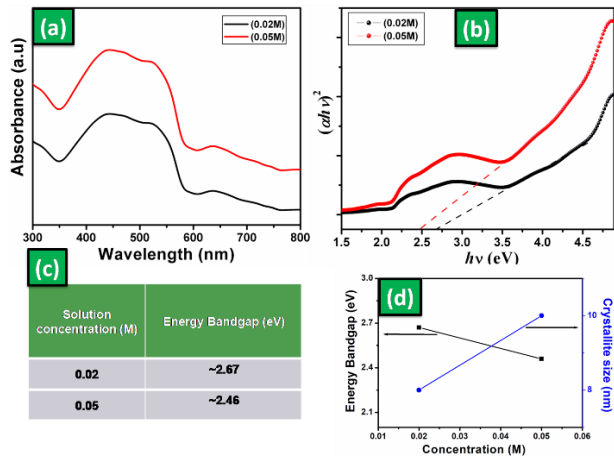
Figure 4. FESEM images of α -Fe₂O₃ nanoparticles calcined at 400 °C for 2 h with various concentration of (a) 0.01 M (b) 0.02 M, (c) 0.05 M, and (d) table showing the variation of grain size with concentration.



Figures 4(a-c) show FESEM images of the calcined samples at 400 °C for 2 h of α -Fe₂O₃ with a concentration of 0.01, 0.02, and 0.05 M, respectively. Well dispersed spherical nanoparticles with diameter of ~6 nm were obtained for α -Fe₂O₃ with 0.01 M (see Figure 4(a)). By increasing solution concentration, size of the α -Fe₂O₃ particles was

found to increase to ~8 nm for 0.02 M (see Figure 4(b)), ~10 nm for 0.05 M (see Figure 4(c)), respectively. The different solution concentration of iron precursor resulted to increase size of α -Fe₂O₃ while keeping the experimental conditions fixed for all the samples.

Figure 5. (a) UV-Vis absorption spectra of α -Fe₂O₃ nanoparticles calcined at 400 °C for 2 h, (b) corresponding energy bandgap plot, (c) table showing the variation of bandgap with concentration, and (d) Plot of energy bandgap and crystallite size as a function of concentration.

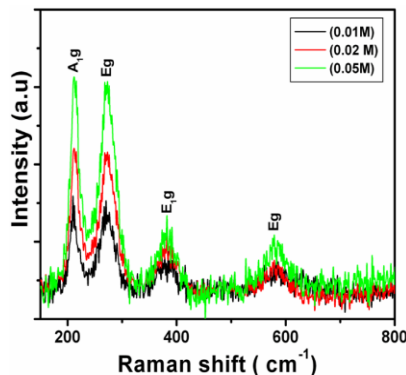


Optical properties of the prepared samples have been studied by UV-visible absorption spectra as shown in Figure 5 (a). It has been obviously obtained from the figure that the absorption peaks demonstrated a red shift as the size of the nanoparticles increased with the increase of concentration. The energy band-gap of α -Fe₂O₃ nanoparticles was obtained by using this equation (Parida *et al.*, 2011).

$$\alpha h\nu = A(h\nu - E_g)^n \quad (1)$$

where α is a well know coefficient of absorption, A is constant, ν is the light frequency, E_g is defined as the energy band-gap, h is Planck's constant and n is the transition kind of the semiconductor. The optical band gap was found by plotting $(\alpha h\nu)^2$ vs. $h\nu$. Figure 5(b) represents the plot of band-gap of α -Fe₂O₃ nanoparticles with various concentrations. The energy bandgap of α -Fe₂O₃ with 0.02 M and 0.05 M concentration are 2.67 and 2.46 eV, respectively, showing a clear red shift as the sizes increased. Therefore, a comparison to the bulk obtained value α -Fe₂O₃ (2.2 eV) (Zhu *et al.*, 2012), shows that the absorption band edge optically for the α -Fe₂O₃ shows red shift with reference to that of the bulk α -Fe₂O₃. This shift might be ascribed to the clear effect of quantum size (Brus, 1996) which resulted from the α -Fe₂O₃ nanoparticles. Figure 5(d) shows that the bandgap value decreased and the size increased with the increase of solution concentration.

Figure 6. Room temperature Raman spectra of α -Fe₂O₃ nanoparticles calcined at 400 °C for 2 h with various concentration.



To understand the quality and confirm crystal phases of α -Fe₂O₃ nanoparticles, structure sensitive Raman spectroscopic measurements have been performed. Figure 6 showed the Raman spectra of α -Fe₂O₃ nanoparticles which recorded at room temperature. The most familiar iron oxide on earth is α -Fe₂O₃ nanoparticles which crystallized in a corundum-type structure. In the standard Raman spectrum of α -Fe₂O₃, the expected phonon lines are seven in which two A_{1g} modes and five E_g modes are well known (Chen *et al.*, 2010). It is clear from figure 6 that the peaks that appear in the spectra of α -Fe₂O₃ nanoparticles with 0.01 M concentration at 212, 271, 386, and 580 cm⁻¹ connected with the specific peaks of α -Fe₂O₃, i.e. the peak positioned at 212 cm⁻¹ relate to the A_{1g} mode. The three peaks at about 271, 386 and 580 cm⁻¹ are attributed to the E_g mode (Chen *et al.*, 2010). Nevertheless, with the increase in concentration, some shifts towards higher wavenumbers were evidenced which might be due to increase in size of the nanoparticles. These findings concluded that a highly crystalline α -Fe₂O₃ can be easily produced by one-step sonication method.

4. Conclusion

In summary, an easy, cost-effective and environmentally benign sonication process has been used to prepare α -Fe₂O₃ nanoparticles with tunable size in quantum confinement range. FESEM images showed that the prepared samples were in quantum regime, and the size of the nanoparticles increased from 4 nm to 11 nm with the increase value in concentration from 0.01 M to 0.05 M. XRD and Raman results revealed that α -Fe₂O₃ nanoparticles possessed crystalline nature with rhombohedral symmetry. The optical appearance properties demonstrated that the energy band-gap of the α -Fe₂O₃ nanoparticles decreased from 2.67 to 2.46 eV associated with the increase value in concentration resulted to an obvious red shift. Finally, the current study concluded that the possibility to tune the particles size, energy band gap, and the crystallinity of α -Fe₂O₃ nanoparticles have been achieved by using a simple and cost effective sonication method. This method might be useful for preparing magnetic and non-magnetic nanostructures with tunable properties for optical applications.

Bios

Adil Alshoabi

Department of Physics, College of Science, King Faisal University, Al Ahsa, Saudi Arabia, adshoabi@kfu.edu.sa, 00966506933370

Dr Al shoabi is a Sheffield graduate, assistant professor, Chairman of Department of Physics, Mathematics and Statistics, and General Supervisor of KFU Central laboratories. He has published 32 ISI/Scopus-indexed articles. His research interest is a blend of the Chemistry, Physics and Engineering of Inorganic Materials, especially oxides, which focuses on materials with interesting and/or useful electrical properties, especially ionic conductors, mixed ionic/electronic conductors, semiconductors, ferro- and di-electrics. ORCID: 0000-0002-9548-6503

Acknowledgments

This work was supported by a Research Grant from King Faisal University.

References

Ahmed, F., Arshi, N., Anwar, M.S., Danish, R. and Koo, B.H. (2014). Quantum-confinement induced enhancement in photocatalytic properties of iron oxide nanoparticles prepared by ionic liquid. *Ceramics International*, 40(10), 15743–51.

- Bondarchuk, A.N., Peter, L.M. and Kissling, G.P. (2017). Vacuum-annealing induces subsurface redox-states in surfactant-structured a-Fe₂O₃ photoanodes prepared by ink-jet printing. *Applied Catalysis B: Environmental*, **211**(n/a), 289–95.
- Brus, L. (1986). Electronic wave functions in semiconductor clusters: Experiment and theory. *The Journal of Physical Chemistry*, **90**(12), 2555–60.
- Chen, H. M., Zhao, Y. Q., Yang, M. Q., He, J. H., Chu, P. K., Zhang, J. and Wu, S. H. (2010). Porous α -Fe₂O₃ nanospheres with excellent gas-sensing properties. *Analytica Chimica Acta*, **659**(1-2), 266–73.
- Chen, L., Yang, X. Liu, J., Wu, H., Zhan, H. and Liang, C. and Wu, M. (2010). Continuous shape- and spectroscopy-tuning of hematite nanocrystals. *Inorg. Chem*, **49**(18), 8411–20.
- Cherian, C. T., Sundaramurthy, J., Kalaivani, M., Ragupathy, P., Kumar, P. S., Thavasi, V., Reddy, M. V., Sow, C. H., Mhaisalkar, S. G., Ramakrishna, S. and Chowdari, B. V. R. (2012). Electrospun α -Fe₂O₃ nanorods as a stable, high capacity anode material for Li-ion batteries. *J. Mater. Chem.*, **22**(n/a), 12198–204.
- Horak, D., Pustovyv, V., Babinskyi, A., Palyvoda, O.M., Chekhun, V.F., Todor, I. and Kuzmenko, O. (2017). Enhanced antitumor activity of surface-modified iron oxide nanoparticles and an a-tocopherol derivative in a rat model of mammary gland carcinosarcoma. *International Journal of Nanomedicine*, **12**(n/a), 4257–68.
- Ibrahim, E.M.M., Abdel-Rahman, L. H., Abudief, A. M., Elshafaie, A., Hamdan, S. K. and Ahmed, A. M. (2018). Electric, thermoelectric and magnetic characterization of γ -Fe₂O₃ and Co₃O₄ nanoparticles synthesized by facile thermal decomposition of metal-Schiff base complexes. *Materials Research Bulletin*, **99**(n/a), 103–8.
- Khabiri, G., Aboaraia, A.M., Soliman, M., Guda, A.A., Butova, V.V., Yahia, I.S. and Soldatov, A.V. (2020). A novel α -Fe₂O₃@MoS₂QDs heterostructure for enhanced visible-light photocatalytic performance using ultrasonication approach. *Ceramics International*, **46**(11), 19600–8.
- Khatami, M., Alijani, H.Q., Fakheri, B., Mobasseri, M.M., Heydarpour, M., Farahani, Z.K. and Khan, A.U. (2019). Super-paramagnetic iron oxide nanoparticles (SPIONs): greener synthesis using Stevia plant and evaluation of its antioxidant properties. *Journal of Cleaner Production*, **208**(n/a), 1171–7.
- Kopanja, L., Milosevic, I., Panjan, M., Damjanovic, V. and Tadic, M. (2016). Sol-gel combustion synthesis, particle shape analysis and magnetic properties of hematite (a-Fe₂O₃) nanoparticles embedded in an amorphous silica matrix. *Applied Surface Science*, **362**(n/a), 380–6.
- Li, Y.Z., Cao, Y.L., Jia, D.Z., Wang, Y. and Xie, J. (2014). Solid-state chemical synthesis of mesoporous a-Fe₂O₃ nanostructures with enhanced xylene-sensing properties. *Sensor. Actuator. B Chem*, **198**(198), 360–5.
- Lubis, S., Maulana, I. and Masyithah, M. (2018). Synthesis and characterization off TiO₂/ α -Fe₂O₃ composite using hematite from iron sand for photodegradation removal of dye. *Jurnal Natural*, **18**(1), 3–43.
- Mufti, N., Atma, T., Fuad, A. and Sutadji, E. (2014). Synthesis and characterization of black, red and yellow nanoparticles pigments from the iron sand. *AIP Conference Proceedings*, **1617**(n/a), 165–9.
- Parida, K.M., Nashim, A. and Mahanta, S.K. (2011). Visible light driven Gd₂Ti₂O₇/GdCrO₃ composite for hydrogen evolution. *Dalton Transactions*, **40**(48), 12839–45.
- Patil, P.B., Parit, S.B., Waifalkar, P.P., Patil, S.P., Dougale, T.D. and Sahoo, S.C. (2018). PH triggered curcumin release and antioxidant activity of curcumin loaded g-Fe₂O₃ magnetic nanoparticles. *Materials Letters*, **223**(n/a), 178–81.
- Patil, R.M., Thorat, N.D., Shete, P.B., Bedge, P.A., Gavde, S., Joshi, M.G., Tofail, S.A.M. and Bohara, R.A. (2018). Comprehensive cytotoxicity studies of superparamagnetic iron oxide nanoparticles, *Biochem. Biophys. Rep.*, **13**(n/a), 63–72.
- Qiu, G., Huang, H., Genuino, H., Opembe, N., Stafford, L., Dharmarathna, S. and Suib, S.L. (2011). Microwave-assisted hydrothermal synthesis of nanosized α -Fe₂O₃ for catalysts and adsorbents. *J. Phys. Chem. C*, **115**(40) 19626–31.
- Ramalingam, V., Harshavardhan, M., Kumar, S.D. and devi, S. M. (2020). Wet chemical mediated hematite a-Fe₂O₃ nanoparticles synthesis: Preparation, characterization and anticancer activity against human metastatic ovarian cancer. *Journal of Alloys and Compounds*, **834**(5), 155118–28.
- Rasheed, R. and Meera, V. (2016). Synthesis of iron oxide nanoparticles coated sand by biological method and chemical method. *Proc. Technol*, **24**(n/a), 210–6
- Ren, G., Wang, X., Zhang, Z. and Wang, X.L. (2017). Characterization and synthesis of nanometer magnetite black pigment from titanium slag by microwave-assisted reduction method. *Dyes Pigments*, **147**(n/a), 24–30.
- Ryan, M.J., Kney, A.D. and Carley, T.L. (2017). A study of selective precipitation techniques used to recover refined iron oxide pigments for the production of paint from a synthetic acid mine drainage solution. *Appl. Geochem*, **79**(n/a), 27–35.
- Sivakumar, S., Anusuya, D., Khatiwada, C.P., Sivasubramanian, J. and Venkatesan, A. (2014). Characterizations of diverse mole of pure and Ni-doped a-Fe₂O₃ synthesized nanoparticles through chemical precipitation route. *Spectrochimica Acta Part A: Molecular and Biomolecular Spectroscopy*, **128**(n/a), 69–75.
- Tao, Y., Jiang, B., Yang, X., Ma, X., Chen, Z., Wang, X. and Wang, Y. (2020). Physicochemical study of the sustainable preparation of nano-Fe₂O₃ from ferrous sulfate with coke. *Journal of Cleaner Production*, **255**(n/a), 120175–84
- Wang, Z. Y., Zhou, L. and Lou, X. W., (2012). Metal oxide hollow nanostructures for lithium-ion batteries. *Adv. Mater.*, **24**(14), 1903–11.
- Widayat, W., Putra, D.A. and Nursafitri, I. (2019). Preparation of Fe₂O₃-Al₂O₃ Catalysts and Catalytic Testing for Biodiesel Production. *Materials Today: Proceedings*, **13**(n/a), 97–102.
- Xia, Y. N., Xiong, Y. J., Lim, B. and Skrabalak, S. E. (2009). Shape-controlled synthesis of metal nanocrystals: Simple chemistry meets complex physics. *Angew. Chem., Int. Ed.*, **48**(1), 60–103.
- Xia, Y., Chen, H., Hu, S., Sun, J., Zhang, F. and Gu, N. (2018). Effects of nano α Fe₂O₃ on proliferation, osteogenic differentiation and mineral synthesis of dental pulp stem cells. *J. Southeast Univ.*, **48**(1), 165–9.
- Xu, X., Cao, C. and Zhu, Y. (2015). Facile synthesis of single crystalline mesoporous hematite nanorods with enhanced supercapacitive performance. *Electrochimica Acta*, **155**(n/a), 257–62.
- Zhou, M.J., Zhou, S.Z., Pang, X.C., Li, K.R. and Qiao, X.G. (2020). Preparation of superparamagnetic γ -Fe₂O₃@LS@PS composite latex particles through pickering miniemulsion polymerization. *Colloids and Surfaces A: Physicochemical and Engineering Aspects*, **585**(n/a), 124040–6.
- Zhu, H. Y., Jiang, R., Xiao, L. and Li, W. (2010). A novel magnetically separable gamma-Fe₂O₃ /crosslinked chitosan adsorbent: preparation, characterization and adsorption application for removal of hazardous azo dye. *Journal of Hazardous Materials*, **179**(1-3), 251–7.
- Zhu, L.P., Bing, N.C., Wang, L.L., Jin, H.Y., Liao, G.H. and Wang L.J. (2012). Synthesis, growth mechanism, and their application in photocatalysis. *Dalton Transactions*, **41**(10), 2959–65.